2023 IEEE International Conference on Robotics and Automation (ICRA 2023)
May 29 - June 2, 2023. London, UK

Twist Snake: Plastic table-top cable-driven robotic arm with all motors located at the base link

Kazutoshi Tanaka[1] and Masashi Hamaya[1]

***Abstract*— Table-top robotic arms for education and research must be low-cost for availability and lightweight and soft for safety. Therefore, as such a robot, this study focuses on designing a plastic table-top cable-driven robotic arm with all motors located at the base link. However, locating all motors at the base link results in a significant distance between a driving motor and driven joint, increases the number of parts for the force transmission, and increases the risk of a cable loosening and coming off of a pulley. To overcome these issues, this study proposed a novel cable-driven robotic arm named Twist Snake. We designed a joint composition of Twist Snake to minimize the number of parts for the force transmission. In addition, it has a compact cable-pretension/termination-mechanism and covering parts to prevent the cable from loosening and coming off of the pulley. The arm comprised 475 mm long moving links with an 802 g. The feasibility of the arm was experimentally demonstrated by contact rich tasks, the insertion of a toy peg into a hole and swiping a whiteboard with a cleaner. The optimization of the proposed design and the development of a learning method for the arm that leverages contact will be investigated in future work.**

I. INTRODUCTION

Table-top robotic arms for education and research [1], [2] must be low-cost for availability and lightweight and soft for safety. Manzoor *et al.* presented an open-source educational platform robotic arm [3]. Quigley *et al.* proposed a low-cost robotic arm for research [4]. In this study, we design a low-cost, lightweight, and soft table-top robotic arm.

A cable-driven robot has lightweight and compact moving links via the removal of motors from the links and touches an object softly without damaging it owing to the elasticity of a cable. Therefore, various cable-driven robots have been developed such as humanoid [5], 10–20 m long robotic arms [6], [7], hands [8], [9], [10], continuum arms [11], [12], [13], [14], and exoskeletons [15], [16]. In addition, these robots have been used widely in applications such as the retrieval of fuel debris [7], table tennis [17], clothing assistance [18], rehabilitation [19], [20], and surgery [21]. Locating all motors of a cable-driven robotic arm at the base link further decreases the weight of the moving links. Endo *et al.* demonstrated a cable-driven robotic arm with 10 m long moving links, weighing 49.9 kg, and locating all motors at the base link [7]. Generally, a cable-driven robotic arm with all motors located at the base link is referred to as a snake-arm robot. The use of plastic structural parts in the moving links of a cable-driven robotic arm also decreases the weight and cost of the links. Tanaka *et al.* used a carbon fiber reinforced plastic (CFRP) to design cylinder tubes for a pneumatic humanoid robot instead of aluminum tubes, which jumped and hit a ball in the air [22]. However, locating all motors at the base link results in a significant distance between a driving motor and a driven joint, increases the number of parts for the force transmission, and increases the risk of the cable loosening and coming off of a pulley. In addition, using plastic structural parts increases the risk of coming off because plastic structural parts are easily bent by the actuating force.

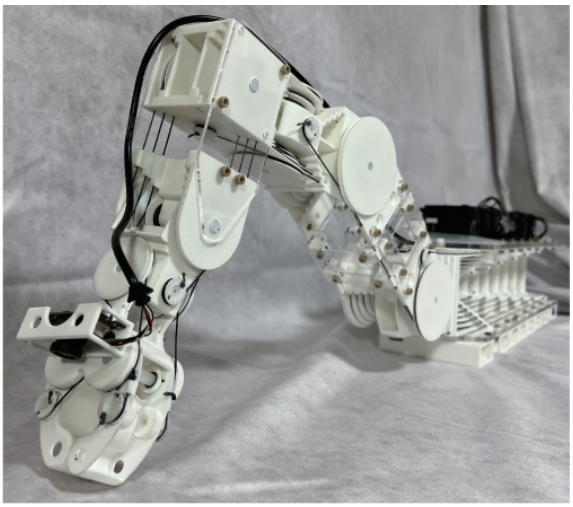

Fig. 1. Twist Snake: a plastic table-top cable-driven robotic arm with all motors located at the base.

To this end, we developed a novel cable-driven robotic arm as shown in Fig. 1, which is a plastic table-top cable-driven robotic arm with all motors located at the base link equipped with the following features to overcome the aforementioned limitations. The first feature is a joint composition to minimize the number of parts for force transmission by simplifying the cable running paths. The second is a cable-pretension/termination-mechanism to prevent the cable from loosening and coming off of a pulley. The third is covering parts around the cable in joint parts to avoid this coming off of a pulley. Finally, the fourth is a camera on the gripper of the arm to estimate the pose of the arm. We named the developed arm as Twist Snake because it is a snake-arm robot that largely twists its gripper by rotating one joint, unlike most of other snake-arm robots that do not due to their joint composition.

[1]Kazutoshi Tanaka and Masashi Hamaya are with OMRON SINIC X Corporation, Hongo 5-24-5, Bunkyo-ku, Tokyo, Japan kazutoshi.tanaka@sinicx.com

*This work was supported by JSPS KAKENHI Grant Number JP19K14936 and JST, PRESTO Grant Number JPMJPR22C6, Japan.

II. Related works

A. Cable-driven robots

Various cable-driven robotic arms have been developed. The Barrett WAM is a commercially available cable-driven robotic arm [23]. Bücher *et al.* developed a high-speed cable-driven robotic arm actuated using pneumatic artificial muscles [24]. Quigley *et al.* proposed the design of a low-cost cable-driven robotic arm as a platform for research on learning robotic manipulation [4]. Kim proposed a cable-driven robotic arm for high-speed and safe interaction with humans [25]. Tsumaki *et al.* presented an anthropomorphic cable-driven robotic arm with seven degrees-of-freedom [26]. These cable-driven robotic arms were actuated by both motors at the base link and motors at the moving links; however, we focus on a cable-driven robotic arm that locates *all* motors at the base link.

B. Cable-driven arm with all motors located at the base link

In several robots, all motors have been located at the base link to minimize the weight of their moving links. Takeichi *et al.* presented a 20 m long cable-driven robotic arm with a balloon body [7]. Endo *et al.* developed a 10 m long cable-driven robotic arm to retrieve fuel debris [7]. Li and Du presented a compact continuum robot that controlled the position of the end effector accurately [13]. Qin *et al.* also demonstrated a snake-inspired continuum robot with universal joints for ease of control [12]. Inspired by these arms, in our cable-driven robotic arm, all motors are located at the base link to minimize the weight of the moving links. However, when designing our arm, we considered minimizing the number of parts for the force transition and the joint composition as a table-top arm to reach the gripper to board positions on the table. Owing to the joint composition, Twist Snake largely twists its gripper by rotating one joint unlike the other snake-arm robots without such a joint that cannot twist one.

C. Pose estimation from partial sensory information

Researchers presented methods for estimating the pose of a soft robotic arm from partial sensory information. Thuruthel *et al.* proposed a method for estimating the tip position and touching force of a soft pneumatic actuator using embedded bending sensors and a long-short-term-memory (LSTM) network [27]. Van Meerbeek *et al.* developed a method for detecting the deformation type of a soft arm from sensors made of internally illuminated elastomer foam [28]. Soter *et al.* proposed a method for estimating the visual image of a soft robotic arm obtained from bending sensors using a stacked convolutional autoencoder (CAE) and a recurrent neural network (RNN) when using one type of commands [29]. Tanaka *et al.* demonstrated another method for estimating the positions of a center line of a soft robotic arm on a visual image obtained from bending sensors using reservoir computing when using multiple types of commands [30]. Inspired by these works, our arm estimates its pose based on partial sensor information. However, in contrast to these works using embedded sensors to estimate the pose, our arm employed a camera on the gripper of the arm to estimate the pose.

TABLE I
Specification of the arm

Motor	Dynamixel MX-64/106 (ROBOTIS)
RBG camera	BSW505MBK (BAFFALO)
Material	Nylon, Acrylic plates
Moving part weight	802 g
Total weight	2650 g
Base size	100x392x145.5 mm (WxDxH)
Total size	100x867x145.5 mm (WxDxH)

D. Cable-pretension/termination-mechanism

Cable-pretension-mechanisms have been proposed to add tension to the cable and avoid slacking and coming off of the pulley. Cherelle *et al.* presented an actuator named MACCEPA [31], and Vanderborght *et al.* proposed another actuator called MACCEPA 2.0 [32] as mechanisms that pull or reel a cable to add pretension to this cable and change the stiffness of a spring. Böttcher *et al.* used a sliding mechanism to add pretension to a cable in their parallel continuum robot [33]. Yeshmukhametov *et al.* presented a cable-pretension-mechanism that pushed a cable [34]. Liu *et al.* used a sliding part in a linkage as a cable-pretension-mechanism in their cable-driven redundant spatial arm [35]. These mechanisms require space for the parts to move and add pretension; however, in our mechanism, pretension is added by reeling a cable without the spatial requirement such as the wire-clamping mechanism in the high-speed robotic arm [25].

A cable-termination-mechanism fixes the cable of a robotic arm compactly and rigidly. Horigome *et al.* proposed a cable-termination-mechanism for fixing a synthetic fiber cable using a grooved pulley and pin [36]. Gerez and Liarokapis proposed a compact cable-termination-mechanism using a ratchet and clutch [37]. A pulley in these mechanisms reels a cable and adds tension to this cable while another part stops this pulley. In our mechanism, a pulley also reels a cable to compactly add tension and fix this cable by stopping and fixing the pulley to the joint part with a hexagonal pin.

III. Design of Twist Snake

A. Overview

Fig. 1 depicts Twist Snake. Table I lists the specifications of Twist Snake. The arm has six joints in its arm and one joint in its gripper. The gripper driven by motors at the base link via cables is a feature of Twist Snake. The weight and length between the end of the gripper and the axis of the Joint1 were 802 g and 475 mm, respectively. The total weight and length of the arm were 2650 g and 867 mm, respectively.

The structural parts of Twist Snake were made from plastic. These were 3D-printed nylon parts and acrylic boards cut using a laser cutter. The thicknesses of the acrylic boards in the upper arm, front arm, and the base were 2, 2, and 5

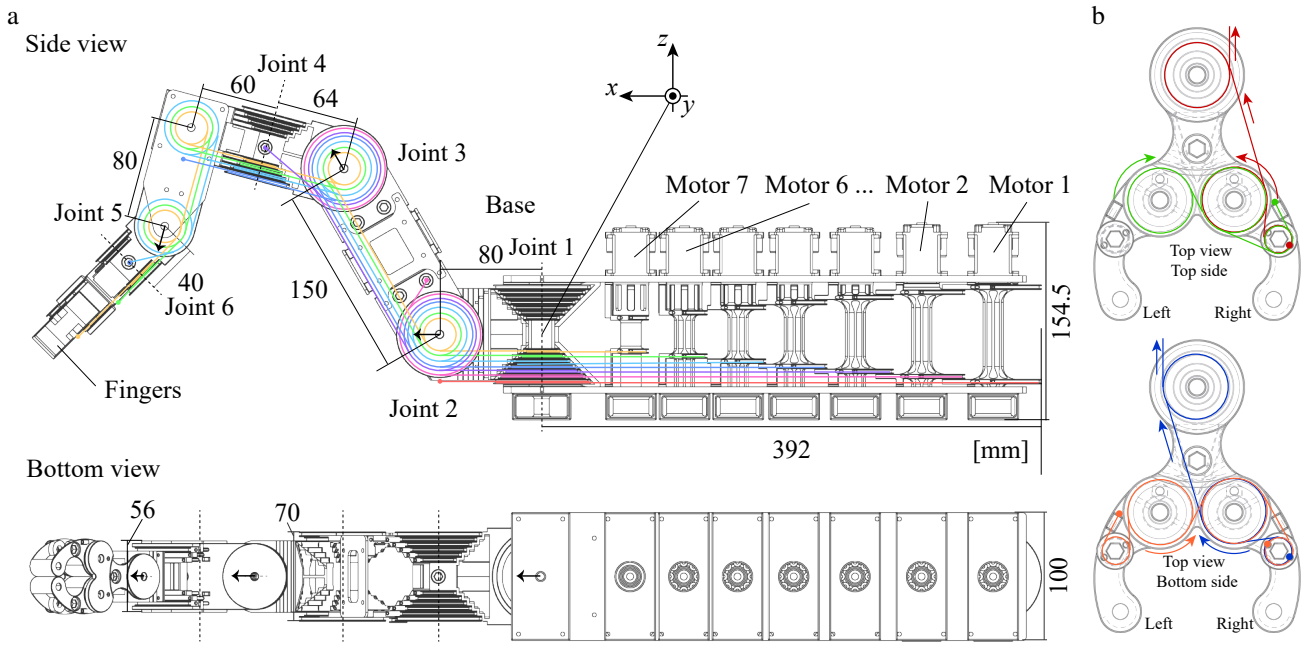

Fig. 2. Schematic of (a) overall arm and (b) gripper. Lines with a color represent cables. One of the cables is pulled by a motor, goes through multiple joints, and pulls a joint (a). Only cables running to the bottom side of the base link are shown in (a). The other cables running the top side are not shown in (a) for a clear illustration of the cable pathways. Two cables move the right finger, and the other two cables synchronize the motion of the left finger to the right finger (b).

mm, respectively. Screws and nuts made of polyether-ether-ketone (PEEK) resin connected the nylon parts to acrylic ones. In addition, the joint axes were nylon rods with a diameter of 6 mm. The cable was composed of Dyneema®, an ultra-high molecular weight polyethylene. Further, the diameter of the cable was 0.8 mm with a load capacity of 100 kg.

B. Joint composition

Fig. 2a shows the motors and the joint composition of Twist Snake. Seven servo motors were used to drive the arm via cables. Joint1 and Joint2 required higher torque than the other joints to move the entire moving links of the arm and were moved by motors with a higher output (Dynamixel MX-106). Two pulleys and one axis were attached to each motor and were manufactured as one nylon 3D print part to reduce the number of parts.

The range of motion of all joints of Twist Snake was -90–90 °. Fig. 2a shows the black vectors at the joints that represent the directions of a link when its joint angle is 0 °. Such a wide range enables the arm to reach wide positions on the table.

Fig. 2a shows the path of the cables of the arm. The cables go through pulleys of multiple joints. In other cable-driven arms [4], [25], many small pulleys have been used for the cable to pass through multiple joints. These pulleys required many axes and increased the number of parts and the weight of the arm. In addition, the small radius of the pulleys increases the fatigue in a cable. Thus, in our arm, multiple pulleys shared one joint axis to minimize the parts for the force transmission, as illustrated in Fig. 2. One of the pulleys that shared the same joint axis rotated independently of the other pulleys and one cable passed through one pulley.

One axis of a joint in Twist Snake except for Joint3 was perpendicular to another axis of the previous joint as shown in Fig. 2a. This is because the cable passed straight from a pulley at the previous joint to another pulley at the next joint. Twist Snake included Joint4 to twist the gripper, which is important for a table-top robotic arm to execute manipulations such as rotating a screw and opening a bottle. In contrast to a long robotic arm [7] and a continuum arm [13], a table-top arm needs this joint to move an object in various directions when manipulating the object on a table. Pulleys between Joint4 and Joint5 rotate freely with the forearm link, which is used to receive cables that go straight from Joint4 and send the cables to Joint5.

C. Gripper driven by cables

Fig. 2b shows the cable in the gripper. Four cables were used drive the gripper. The cables that connected to a motor opened the right finger (red) and closed the finger (blue). The right and left fingers open and close simultaneously via the pulling of the cables (green and orange).

While we designed a gripper wherein two fingers rotate in this study, other gripper types can be used by adding any mechanism and cables such as a parallel gripper, a three-finger gripper, and a gripper with multiple DOFs in each finger.

D. Pulleys for going through a joint

Fig. 3 shows the pulleys in Joint2 and the bearings for the pulleys. The thickness of the pulleys was 4 mm. The thickness was mainly determined by the 2 mm width of the

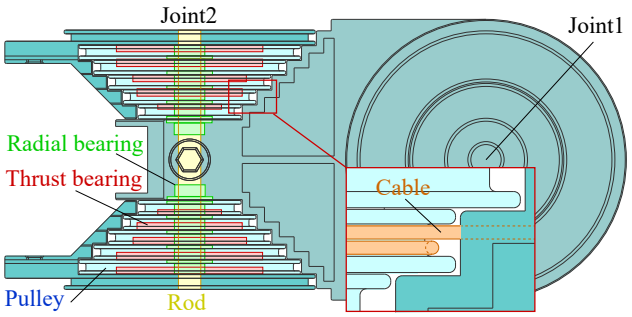

Fig. 3. Multiple pulleys share one joint axis. Radial bearings are inserted between the rod and pulleys and thrust bearings are piled between pulleys to ensure their smooth movement. The cable runs around the pulley and is covered with a joint part.

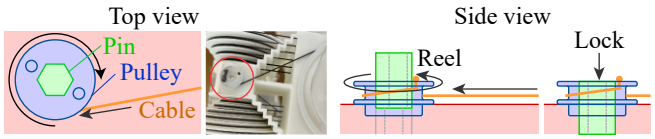

Fig. 4. Cable-pretension/termination-mechanism. A red circle shows the mechanism of a link. The orange line represents the cable. The orange dot represents the knot to fix the cable to the pulley.

groove of the pulleys, which is larger than twice the diameter of the cable. Each cable goes around a pulley approximately once to avoid coming off because the tension for coming off often occurs if a cable does not go around the pulley once, and the cable is rolled up on this cable if a cable goes around the pulley multiple times. We set the differences in the radius of multiple pulleys to 12, 16,..., 36 mm to match the thickness of the pulleys such that a cable could pass straight from a pulley of one joint to another pulley of the next joint with an axis that was perpendicular to the axis of the previous joint.

The pulleys were piled and shared one joint axis as shown Fig. 3. We used oil-less bushes as radial bearings between the pulleys and the rod. The bearings aid in the smooth rotation of the pulleys. Thus, the pulleys rotate around the joint axis and also move in other directions owing to the low stiffness of the plastic parts of the arm, such as the pulleys, bearings, and the rod. Therefore, we placed the pulleys between parts of a joint such that one section of the parts pushed the pulley against other parts to restrict the movement of the pulley in other directions except for rotation. We used oil-less washers as thrust bearings between the pulleys. The radial bearings and the thrust bearings were made of polyacetal resin.

E. Cable-cover-mechanism

The structural parts of the arm often bend owing to the low stiffness of these parts, which causes the cables to come off of the pulley. Therefore, joint parts cover the cables around the pulleys such that the cables pass through the joint as shown in Fig. 3.

F. Cable-pretension/termination-mechanism

Fig. 4 shows the cable-pretension-mechanism to add pretension to a cable and avoid being slack and coming off

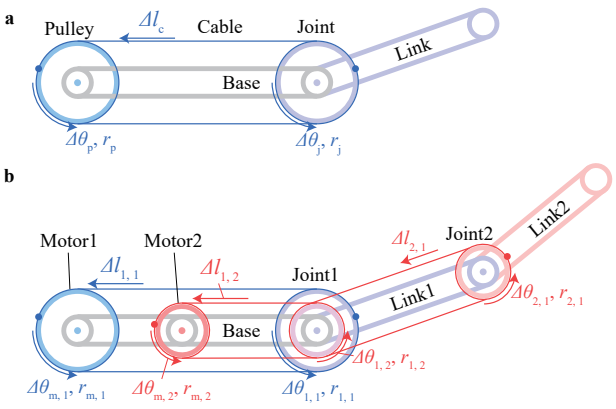

Fig. 5. (a) Cables, a joint, and a pulley. This pulley reels and pulls a cable, which pulls and rotates the joint. (b) The velocity of cable and joints. Blue and red lines represent the cables of Joint1 and Joint2, respectively. Dots represent the fixed point of the cables.

the pulley. Using additional pulleys to push a cable and add tension as shown in other cable-driven robotic arms requires additional spaces to move these pulleys and increases the number of parts and weight of the arm. Thus, we adopted a cable-pretension-mechanism to the arm, wherein the pulley reeled the cable, which was fixed by being inserted a hexagonal Duracon® pin, as shown in the figure. This mechanism is also a cable-termination-mechanism and compact.

The ends of the cables pass into the hole at the pulley of the motor and the hole at the pulley of a cable-pretension/termination-mechanism as shown in Fig. 4. They then terminate by stopping the knot of the cable at the end of the hole. The knot of the cable detaches from the holes to avoid breakage of the structural parts of the arm when an oversized force is provided to a link and oversized tension is applied to the cable.

IV. Control of Twist Snake

A. Position control of the gripper

Twist Snake controls the pose of its gripper $\mathbf{r}_\mathrm{g}$ by changing the target velocity of its motors $\Delta\theta_\mathrm{m}$ as follows. At first, the arm observes $\mathbf{r}_\mathrm{g}$ from the camera on the gripper. Next, it calculates the target velocity of the gripper $\Delta\mathbf{r}_\mathrm{g}$ based on the difference between the observed and target $\mathbf{r}_\mathrm{g}$. Third, it determines the target angular velocity of its joints $\Delta\theta_\mathrm{j}$ from the calculated $\Delta\mathbf{r}_\mathrm{g}$ as $\Delta\theta_\mathrm{j} = J^{-1}\Delta\mathbf{r}_\mathrm{g}$, where J^{-1} is the inverse matrix of the Jacobian matrix. Then, it estimates current joint angles θ_j from observed $\mathbf{r}_\mathrm{g}$ by solving inverse kinematics, and set values in J using estimated θ_j. Finally, it determines $\Delta\theta_\mathrm{m}$ from $\Delta\theta_\mathrm{j}$ as described in Sec. IV-C.

B. An angular velocity of a joint and the previous pulley

Before describing the calculation of the target $\Delta\theta_\mathrm{m}$, we introduce the relationships between an angular velocity of a joint $\Delta\theta_\mathrm{j}$ and that of the previous pulley $\Delta\theta_\mathrm{p}$ using Fig. 5a. This figure shows that the previous pulley reels a cable, which then pulls and rotates the joint. Assuming that there is

no extension and slack of the cables, the velocity of a cable is calculated as

$$\Delta l_{\mathrm{c}} = r_{\mathrm{j}} \Delta\theta_{\mathrm{j}} = r_{\mathrm{p}} \Delta\theta_{\mathrm{p}}, \tag{1}$$

where r, and $\Delta\theta$ represent a radius and angular velocity, and the subscripts $*_{\mathrm{p}}$ and $*_{\mathrm{j}}$ represent the previous pulley and the joint.

C. Target velocity of the motors

We introduce the calculation of the target velocity of the motors using an example shown in Fig. 5b. This figure shows a two-link cable-driven robotic arm driven by two motors at the base link.

Based on Eq. (1), the velocity of cables is calculated as $\Delta l_{1,1} = r_{1,1}\Delta\theta_{1,1} = r_{\mathrm{m},1}\Delta\theta_{\mathrm{m},1}$ and $\Delta l_{1,2} = r_{1,2}\Delta\theta_{1,2} = r_{\mathrm{m},2}\Delta\theta_{\mathrm{m},2}$, where $\Delta\theta$ is an angular velocity of a pulley, and the subscript $*_{i,j}$ represents the j^{th} pulley from the outside at the i^{th} joint.

Link1 rotates at the angular velocity $\Delta\theta_{1,1}$ around Joint1 against the base link. The second pulley from the outside at the first joint Joint1, rotates at $\Delta\theta_{1,2} - \Delta\theta_{1,1}$ against Link1. Therefore, Link2 also rotates at $\Delta\theta_{2,1}$ against the Link1 as

$$\Delta l_{2,1} = r_{2,1}\Delta\theta_{2,1} = r_{1,2}(\Delta\theta_{1,2} - \Delta\theta_{1,1}). \tag{2}$$

From these equations, the angular velocity of the motors, $\Delta\theta_{\mathrm{m},1}$ and $\Delta\theta_{\mathrm{m},2}$ are calculated from the target angular velocity of the joints, $\Delta\theta_{1,1}$ and $\Delta\theta_{1,1}$ as $\Delta\theta_{\mathrm{m},1} = r_{1,1}\Delta\theta_{1,1}/r_{\mathrm{m},1}$ and $\theta_{\mathrm{m},2} = (r_{1,2}\Delta\theta_{1,1} + r_{2,1}\Delta\theta_{2,1})/r_{\mathrm{m},2}$.

As described above using the example of the two link arms, the target velocity of the motors $\Delta\theta_{\mathrm{m},1}, \ldots, \Delta\theta_{\mathrm{m},7}$ are calculated from the target $\Delta\theta_{1,1} \ldots \Delta\theta_{6,6}$ calculated from $\Delta\mathbf{r}_{\mathrm{g}}$ as described in Sec. IV-A and the target angular velocity of the joint in the gripper $\Delta\theta_{7,7}$. We set $r_{1,1} = 36$ mm, $r_{2,1} = 32$ mm, $r_{3,1} = 28$ mm, $r_{4,1} = 24$ mm, $r_{5,1} = 20$ mm, $r_{6,1} = 16$ mm, $i_{7,1} = 12$ mm, and $r_{1,k} = r_{2,k-1} = \ldots = r_{k,1}$ $(k = 1, \ldots, 7)$, as described in Sec. III-B.

Even when the axes of the current and previous joints are perpendicular, such as in Twist Snake, the relationships between the velocity of the cables and the angular velocity of the pulleys do not change.

V. Experiments

We designed experiments to verify whether Twist Snake has the physical performance. We experimentally investigated the basic performance of Twist Snake, such as the response speed, weight capacity, and accuracy of the gripper position control. Moreover, we confirmed that Twist Snake could execute contact-rich tasks such as inserting a peg into a hole and swiping a whiteboard with a whiteboard cleaner, as well as fast-motion tasks such as swinging a table tennis racket. We selected contact-rich and fast-motion tasks to demonstrate the advantages of a cable-driven robotic arm, such as lightweight characteristics and the ability to touch an object gently without damaging it.

We used a motion capture system (V120 Trio, OptiTrack) to measure the pose of the end effector of the arm at 120 Hz instead of the camera at the gripper to focus on the execution accuracy of the actuation system of Twist Snake by removing the camera measurement noise. The control frequency of the arm was 10 Hz.

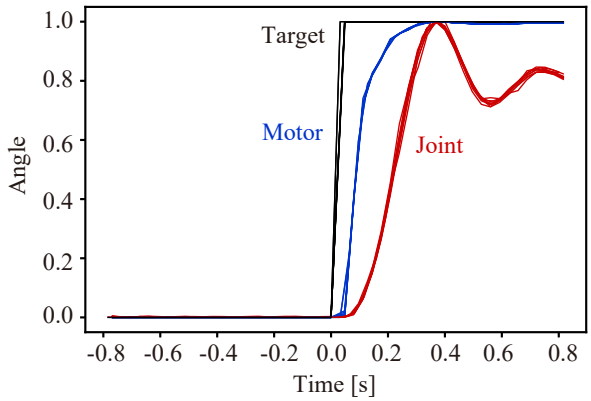

Fig. 6. Response. Black, blue, and red lines represent the target position of the motor, motor angle, and joint angle, respectively. The scale of the target and measured motor positions and the joint angle were converted to the range [0, 1].

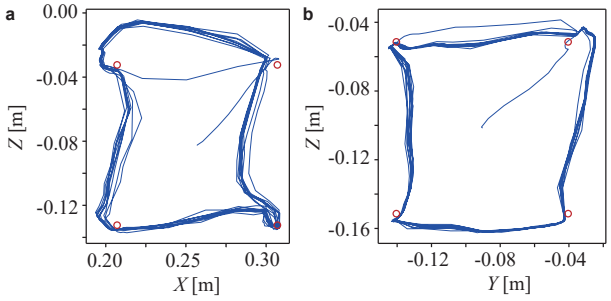

Fig. 7. Point-to-point trajectories in (a) the X-Z plane and (b) the Y-Z plane. Four red points represent the target positions. The blue line represents the positions of the gripper. The coordinates are also shown in Fig. 2.

A. Response speed

We measured the response speed of Twist Snake. The target position of Motor1 was changed by every 2 s from the two target positions 20° apart 20 times.

Fig. 6 shows the response of Joint1 and Motor1. This figure shows that the motor position was reached in 0.4 s, and the joint moved in the same time duration. The motor reached the target position earlier than the joint. We speculated that this could be attributed to the extension of the pulled cable.

B. Weight capacity

We attached a bottle with water to the gripper of the arm via a cable as a load weight. The arm extended the moving links horizontally and moved Joint1 88° to move the links and carry the bottle.

The maximum weight that it could carry was 382 g. The knot to fix a cable to a pulley of a motor detached when it carried a heavier bottle.

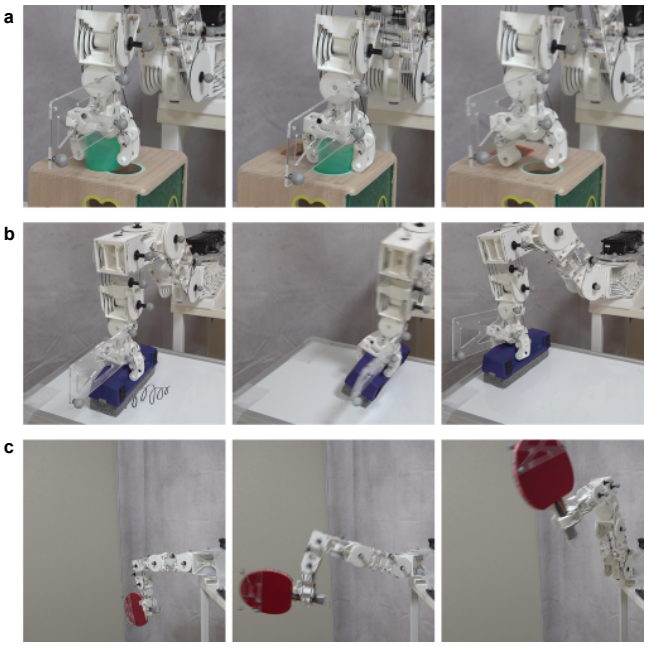

Fig. 8. Snapshots of the arm that executes tasks. (a) Inserting a toy peg into a hole. (b) Swiping a whiteboard and erasing lines. (c) Swinging the table tennis racket. The arm successfully performed contact-rich manipulation tasks and a fast-motion task.

C. Accuracy of the position control

We investigated the accuracy of the position control of the gripper of Twist Snake. At first, we set the target randomly in a box area with the 0.1 m vertices and placed the initial position of the gripper at the center. Second, we also changed the target from the four points in the same order.

The target positions of the motors were sent to and changed the target at 1 s intervals 200 times, and then the gripper pose was measured. Further, the order of the target was changed, and the gripper pose was measured. Thereafter, the difference in the gripper position was calculated.

The mean and standard deviation of the length between the target and actual positions were 4.9 and 2.6 mm, respectively.

We changed the target position of the gripper and measured the motion of the gripper to examine the reaching behavior of the arm. In one trial, we moved the gripper in the X-Z plane while moving in the Y-Z plane in another trial. Fig. 2 shows the coordinate of the arm. The target positions were located at the four vertices of a square with 100 mm edges, wherein the initial positions of the gripper were at the center. We changed the target position 40 times at 2 s intervals.

Fig. 7 shows the trajectories of the positions of the gripper when the target position changed. The figure indicates that the gripper did not move in the accurate direction of the target position; however, the gripper approached each target by feedback control.

D. Tasks execution

We verified the capacity of the arm to execute various tasks. The arm was used to insert a toy peg into a hole and swipe a whiteboard as contact-rich tasks. It was also used to swing a table tennis racket as a fast-motion task. We empirically determined the target position patterns of the gripper when inserting the peg-in-hole and when using the eraser, as well as the target position patterns of the motors when swinging the arm, respectively. Moreover, we attached the marker to the racket and measured the motion of the marker when swinging the arm.

Fig. 8 shows that the arm successfully executed the tasks of the toy peg-in-hole, using a whiteboard eraser, and swinging the arm with a table tennis racket. The speed of the racket reached its peak of 2.4 m/s in 1 s when swinging the racket.

VI. Discussion

The design of Twist Snake can be optimized because we simply set the design parameters simply, such as the same thickness of the pulleys and the same output of the motors. The payload of Twist Snake, namely 852 g, was smaller than the 2.0 kg of the low-cost arm [4] and 3.0 kg of the high-speed arm [25] because a knot to fix a cable detached from a pulley of a motor when Twist Snake carried a heavier object. The design of the cable-termination-mechanism can be optimized to improve the payload considering the maximum cable tension. The required torque of the distal joints such as a joint in the gripper is smaller than that of the proximal joints such as Joint1. Thus, cables with a smaller diameter and thicker pulleys can be used for these distal joints and the size of the joints can be reduced further. Additional motors will enable us to design a more complex arm using the same Twist Snake framework, such as an arm with redundant joints and a gripper with more DOF.

The average position error of Twist Snake was 4.9 mm, as described in Sec. V-B. The error was larger than the 0.153 mm of the high-speed arm [25]. We speculate that the position accuracy of Twist Snake is low owing to the elasticity of the cables, as noted in Sec. V-A. Twist Snake should execute tasks not by depending on its low position accuracy but rather on its advantages such as lightweight and softness as a result of cables. For example, Twist Snake can execute tasks using pose estimation of a grasped object leveraging contact between objects [38], [39] and learning methods for assembly tasks leveraging softness in the body of a robot [40], [41], [42].

VII. Conclusions

We developed the Twist Snake, which is a plastic table-top cable-driven robotic arm with all motors located at the base link, as an education and research platform with low-cost for accessibility and lightness and softness for safety. In future work, we plan to investigate the optimization of the proposed design and development of a learning method for the arm that leverages contact.

References

[1] "OpenMANIPULATOR-X e-manual," https://emanual.robotis.com/docs/en/platform/openmanipulator_x/overview/.
[2] "myCobot," https://www.elephantrobotics.com/en/mycobot-en/.

[3] S. Manzoor, R. U. Islam, A. Khalid, A. Samad, and J. Iqbal, "An open-source multi-dof articulated robotic educational platform for autonomous object manipulation," *Robotics and Computer-Integrated Manufacturing*, vol. 30, no. 3, pp. 351–362, 2014.

[4] M. Quigley, A. Asbeck, and A. Ng, "A low-cost compliant 7-DOF robotic manipulator," in *IEEE International Conference on Robotics and Automation*, 2011, pp. 6051–6058.

[5] Y. Asano, K. Okada, and M. Inaba, "Design principles of a human mimetic humanoid: Humanoid platform to study human intelligence and internal body system," *Science Robotics*, vol. 2, no. 13, p. eaaq0899, 2017.

[6] M. Takeichi, K. Suzumori, G. Endo, and H. Nabae, "Development of giacometti arm with balloon body," *IEEE Robotics and Automation Letters*, vol. 2, no. 2, pp. 951–957, 2017.

[7] G. Endo, A. Horigome, and A. Takata, "Super dragon: A 10-m-long-coupled tendon-driven articulated manipulator," *IEEE Robotics and Automation Letters*, vol. 4, no. 2, pp. 934–941, 2019.

[8] Z. Xu, V. Kumar, and E. Todorov, "A low-cost and modular, 20-DOF anthropomorphic robotic hand: Design, actuation and modeling," in *IEEE-RAS International Conference on Humanoid Robots*. IEEE, 2013, pp. 368–375.

[9] T. Takaki and T. Omata, "High-performance anthropomorphic robot hand with grasping-force-magnification mechanism," *IEEE/ASME Transactions on mechatronics*, vol. 16, no. 3, pp. 583–591, 2010.

[10] S. Shirafuji, S. Ikemoto, and K. Hosoda, "Development of a tendon-driven robotic finger for an anthropomorphic robotic hand," *The International Journal of Robotics Research*, vol. 33, no. 5, pp. 677–693, 2014.

[11] R. J. Webster III and B. A. Jones, "Design and kinematic modeling of constant curvature continuum robots: A review," *The International Journal of Robotics Research*, vol. 29, no. 13, pp. 1661–1683, 2010.

[12] G. Qin, A. Ji, Y. Cheng, W. Zhao, H. Pan, S. Shi, and Y. Song, "A snake-inspired layer-driven continuum robot," *Soft Robotics*, 2021.

[13] Z. Li and R. Du, "Design and analysis of a bio-inspired wire-driven multi-section flexible robot," *International Journal of Advanced Robotic Systems*, vol. 10, no. 4, p. 209, 2013.

[14] F. Renda, M. Giorelli, M. Calisti, M. Cianchetti, and C. Laschi, "Dynamic model of a multibending soft robot arm driven by cables," *IEEE Transactions on Robotics*, vol. 30, no. 5, pp. 1109–1122, 2014.

[15] S. J. Ball, I. E. Brown, and S. H. Scott, "Medarm: a rehabilitation robot with 5DOF at the shoulder complex," in *2007 IEEE/ASME international conference on Advanced intelligent mechatronics*. IEEE, 2007, pp. 1–6.

[16] T. Noda, T. Teramae, B. Ugurlu, and J. Morimoto, "Development of an upper limb exoskeleton powered via pneumatic electric hybrid actuators with bowden cable," in *IEEE/RSJ International conference on intelligent robots and systems*. IEEE, 2014, pp. 3573–3578.

[17] K. Mülling, J. Kober, O. Kroemer, and J. Peters, "Learning to select and generalize striking movements in robot table tennis," *The International Journal of Robotics Research*, vol. 32, no. 3, pp. 263–279, 2013.

[18] T. Tamei, T. Matsubara, A. Rai, and T. Shibata, "Reinforcement learning of clothing assistance with a dual-arm robot," in *IEEE-RAS International Conference on Humanoid Robots*. IEEE, 2011, pp. 733–738.

[19] P. Maciejasz, J. Eschweiler, K. Gerlach-Hahn, A. Jansen-Troy, and S. Leonhardt, "A survey on robotic devices for upper limb rehabilitation," *Journal of neuroengineering and rehabilitation*, vol. 11, no. 1, pp. 1–29, 2014.

[20] R. Gopura, D. Bandara, K. Kiguchi, and G. K. Mann, "Developments in hardware systems of active upper-limb exoskeleton robots: A review," *Robotics and Autonomous Systems*, vol. 75, pp. 203–220, 2016.

[21] K. Xu, J. Zhao, and M. Fu, "Development of the sjtu unfoldable robotic system (surs) for single port laparoscopy," *IEEE/ASME Transactions on Mechatronics*, vol. 20, no. 5, pp. 2133–2145, 2014.

[22] K. Tanaka, S. Nishikawa, R. Niiyama, and Y. Kuniyoshi, "Immediate generation of jump-and-hit motions by a pneumatic humanoid robot using a lookup table of learned dynamics," *IEEE Robotics and Automation Letters*, vol. 6, no. 3, pp. 5557–5564, 2021.

[23] B. Rooks, "The harmonious robot," *Industrial Robot: An International Journal*, vol. 33, no. 2, pp. 125–130, 2006.

[24] D. Büchler, H. Ott, and J. Peters, "A lightweight robotic arm with pneumatic muscles for robot learning," in *IEEE International Conference on Robotics and Automation*, 2016, pp. 4086–4092.

[25] Y.-J. Kim, "Anthropomorphic low-inertia high-stiffness manipulator for high-speed safe interaction," *IEEE Transactions on Robotics*, vol. 33, no. 6, pp. 1358–1374, 2017.

[26] Y. Tsumaki, Y. Suzuki, N. Sasaki, E. Obara, and S. Kanazawa, "A 7-DoF wire-driven lightweight arm with wide wrist motion range," in *IEEE/RSJ International Conference on Intelligent Robots and Systems*, 2018, pp. 1–9.

[27] T. G. Thuruthel, B. Shih, C. Laschi, and M. T. Tolley, "Soft robot perception using embedded soft sensors and recurrent neural networks," *Science Robotics*, vol. 4, no. 26, 2019.

[28] I. Van Meerbeek, C. De Sa, and R. Shepherd, "Soft optoelectronic sensory foams with proprioception," *Science Robotics*, vol. 3, no. 24, 2018.

[29] G. Soter, A. Conn, H. Hauser, and J. Rossiter, "Bodily aware soft robots: integration of proprioceptive and exteroceptive sensors," in *IEEE International Conference on Robotics and Automation*. IEEE, 2018, pp. 2448–2453.

[30] K. Tanaka, Y. Minami, Y. Tokudome, K. Inoue, Y. Kuniyoshi, and K. Nakajima, "Continuum-body-pose estimation from partial sensor information using recurrent neural networks," *IEEE Robotics and Automation Letters*, 2022.

[31] P. Cherelle, V. Grosu, P. Beyl, A. Mathys, R. Van Ham, M. Van Damme, B. Vanderborght, and D. Lefeber, "The maccepa actuation system as torque actuator in the gait rehabilitation robot altacro," in *IEEE RAS/EMBS International Conference on Biomedical Robotics and Biomechatronics*. IEEE, 2010, pp. 27–32.

[32] B. Vanderborght, N. G. Tsagarakis, C. Semini, R. Van Ham, and D. G. Caldwell, "Maccepa 2.0: Adjustable compliant actuator with stiffening characteristic for energy efficient hopping," in *IEEE International Conference on Robotics and Automation*. IEEE, 2009, pp. 544–549.

[33] G. Böttcher, S. Lilge, and J. Burgner-Kahrs, "Design of a reconfigurable parallel continuum robot with tendon-actuated kinematic chains," *IEEE Robotics and Automation Letters*, vol. 6, no. 2, pp. 1272–1279, 2021.

[34] A. Yeshmukhametov, K. Koganezawa, A. Seidakhmet, and Y. Yamamoto, "A novel passive pretension mechanism for wire-driven discrete continuum manipulators," in *IEEE/SICE International Symposium on System Integration*. IEEE, 2020, pp. 1168–1173.

[35] T. Liu, Z. Mu, H. Wang, W. Xu, and Y. Li, "A cable-driven redundant spatial manipulator with improved stiffness and load capacity," in *IEEE/RSJ International Conference on Intelligent Robots and Systems*. IEEE, 2018, pp. 6628–6633.

[36] A. Horigome, G. Endo, A. Takata, and Y. Wakabayashi, "Development of new terminal fixation method for synthetic fiber ropes," *IEEE Robotics and Automation Letters*, vol. 3, no. 4, pp. 4321–4328, 2018.

[37] L. Gerez and M. Liarokapis, "A compact ratchet clutch mechanism for fine tendon termination and adjustment," in *IEEE/ASME International Conference on Advanced Intelligent Mechatronics*. IEEE, 2018, pp. 1390–1395.

[38] F. von Drigalski, K. Tanaka, M. Hamaya, R. Lee, C. Nakashima, Y. Shibata, and Y. Ijiri, "A compact, cable-driven, activatable soft wrist with six degrees of freedom for assembly tasks," in *IEEE/RSJ International Conference on Intelligent Robots and Systems*, 2020, pp. 8752–8757.

[39] F. von Drigalski, K. Hayashi, Y. Huang, R. Yonetani, M. Hamaya, K. Tanaka, and Y. Ijiri, "Precise multi-modal in-hand pose estimation using low-precision sensors for robotic assembly," in *IEEE International Conference on Robotics and Automation*. IEEE, 2021, pp. 968–974.

[40] M. Hamaya, R. Lee, K. Tanaka, F. Von Drigalski, C. Nakashima, Y. Shibata, and Y. Ijiri, "Learning robotic assembly tasks with lower dimensional systems by leveraging physical softness and environmental constraints," in *International Conference on Robotics and Automation*. IEEE, 2020, pp. 7747–7753.

[41] M. Hamaya, F. Von Drigalski, T. Matsubara, K. Tanaka, R. Lee, C. Nakashima, Y. Shibata, and Y. Ijiri, "Learning soft robotic assembly strategies from successful and failed demonstrations," in *IEEE/RSJ International Conference on Intelligent Robots and Systems*, 2020, pp. 8309–8315.

[42] M. Hamaya, K. Tanaka, Y. Shibata, F. Von Drigalski, C. Nakashima, and Y. Ijiri, "Robotic learning from advisory and adversarial interactions using a soft wrist," *IEEE Robotics and Automation Letters*, vol. 6, no. 2, pp. 3878–3885, 2021.